Use of multi-temporal Lidar data to extract changes due to the 2016 Kumamoto earthquake

Fumio Yamazaki*[a], Luis Moya[b], Wen Liu[a]
[a] Graduate School of Engineering, Chiba University, Chiba, Japan 263-8522;
[b] International Research Institute of Disaster Science, Tohoku University, Sendai, Japan 980-0845

ABSTRACT

Extraction of collapsed buildings from a pair of Lidar data taken before and after the 2016 Kumamoto, Japan, earthquake was conducted. Lidar surveys were carried out for the affected areas along the causative faults by Asia Air Survey Co., Ltd. The density of the collected Lidar data was 1.5 - 2 points/m^2 for the first flight on April 15, 2016 and 3 - 4 points/m^2 for the second flight on April 23, 2016. The spatial correlation coefficient of the two Lidar data was calculated using a 101 x 101 pixels window (50 m x 50 m), and the horizontal shift of the April-23 digital surface model (DSM) with the maximum correlation coefficient was considered as the crustal movement by the April-16 main-shock. The horizontal component of the calculated coseismic displacement was applied to the post-event DSM to cancel it, and then the vertical displacement between the two DSMs was calculated. The both horizontal and vertical coseismic displacements were removed to extract collapsed buildings. Then building-footprints were employed to assess the changes of the DSMs within them. The average of difference between the pre- and post-event DSMs within a building footprint was selected as a parameter to evaluate whether a building is collapsed or not. The extracted height difference was compared with the spatial coherence value calculated from pre- and post-event ALOS-2 PALSAR-2 data and the result of field damage surveys. Based on this comparison, the collapsed buildings could be extracted well by setting a proper threshold value for the average height difference.

Keywords: Lidar, the 2016 Kumamoto earthquake, building damage, DSM, change detection, PALSAR-2

1. INTRODUCTION

Information gathering after a large-scale natural disaster is very important in emergency response and recovery activities. But the access to the affected areas is often hindered by the disruption of road networks and telecommunication systems. Thus remote sensing technologies have been employed to assess the extent and degree of various damages [1-5]. Various high-resolution optical and SAR satellites have been in operation in the last decade and they were employed to observe affected areas after major natural disasters, such as the 2011 Tohoku, Japan, earthquake and tsunami [6], the 2011 central Thailand flood [7], and the 2015 Gorkha, Nepal, earthquake [8]. The acquired satellite data provided the information on inaccessible affected areas.

Various aerial surveying technologies have also been developed in the last few decades, such as digital aerial cameras, Lidar (Light detection and ranging), and more recently, unmanned aerial vehicles (UAVs, drones). The images acquired by digital aerial cameras have much higher radiometric resolution than those from analogue cameras, and thus they have been extensively used in recent natural disasters [9]. Lidar is the most costly but the most accurate method to acquire digital surface models (DSMs), and hence it has been used to develop detailed digital elevation models (DEMs) and 3D configuration of buildings [10]. But applications of Lidar for damage detection are still few compared with other remote sensing technologies. The main reason is considered as the lack of Lidar data obtained before a disaster.

A series of earthquakes with Mw7.0 as the main-shock hit Kumamoto prefecture in Kyushu Island, Japan in April 2016 [11]. Among the several remote sensing technologies used to monitor the area affected by the Kumamoto earthquake [12], a pair of Lidar datasets taken before and after the main-shock were available [13, 14]. This kind of dataset is not often available. Therefore, this study explores the potential use of Lidar data to extract collapsed buildings over a wide area. The average of difference between the pre- and post-event DSMs within a building footprint was introduced to evaluate whether a building is collapsed or not. The result was compared with the spatial coherence value calculated from pre- and post-event ALOS-2 PALSAR-2 data and field survey data.

Remote Sensing Technologies and Applications in Urban Environments II, edited by Thilo Erbertseder, Nektarios Chrysoulakis, Ying Zhang, Proc. of SPIE Vol. 10431, 104310B · © 2017 SPIE · CCC code: 0277-786X/17/$18 · doi: 10.1117/12.2278061

2. THE 2016 KUMAMOTO EARTHQUAKE SEQUENCE

A Mw6.2 earthquake hit the Kumamoto Prefecture in Kyushu Island, Japan on April 14, 2016 at 21:26 (JST). A considerable amount of structural damages and human casualties had been reported due to this event, including 9 deaths [11]. The epicenter was located in the Hinagu fault with a shallow depth. On April 16, 2016 at 01:25 (JST), about 28 hours after the first event, another earthquake of Mw7.0 occurred in the Futagawa fault, closely located with the Hinagu fault. Thus, the first event was called as the "foreshock" and the second one as the "main-shock". The epicenters of the both events were located in Mashiki Town (about 33-thousand population), to the east of Kumamoto City (about 735-thousand population). The total number of aftershocks (larger than magnitude 3.5) reached 340 times as of April 30, 2017, one year after the foreshock. This number is the largest among recent inland (crustal) earthquakes in Japan [15].

Figure 1 shows the location of these causative faults and Japanese national GNSS Earth Observation Network System (GEONET) stations in the source area [16]. Note that the GEONET system has about 1,300 stations covering Japan's territory uniformly. The displacement of 75 cm to the east-northeast (ENE) was observed at the Kumamoto station while that of 97 cm to the southwest (SE) was recorded at the Choyo station during the main-shock. These observations validated the right-lateral strike-slip mechanism of the Futagawa fault.

The peak ground acceleration (PGA) and the peak ground velocity (PGV) recorded at the KiK-net seismic network's Mashiki station were 925 cm/s^2 and 92 cm/s in the foreshock while those were 1,313 cm/s^2 and 132 cm/s in the main-shock. These values were quite large among recent earthquake records in Japan. Extensive impacts due to strong shaking and landslides were associated by the Kumamoto earthquake sequence, such as collapse of buildings and bridges, and suspension of road and railway networks [11,12]. A total of fifty (50) direct deaths were accounted by the earthquake sequence, mostly due to the collapse of wooden houses in Mashiki town and landslides in Minami-Aso village.

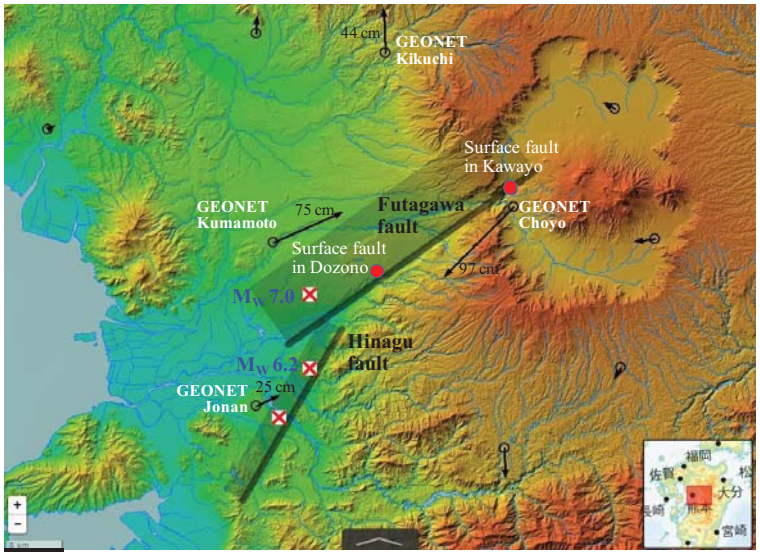

Figure 1. Location of causative faults and GNSS stations in the 2016 Kumamoto earthquake.

3. STUDY AREA AND DATASET

After the foreshock, a Lidar surveying flight was carried out during 15:00 – 17:00 (JST) on April 15, 2016, in order to record the effects of the earthquake [13]. It produced point clouds with an average point density of 1.5-2 points/m^2. Subsequently, because the unexpected main-shock occurred, a second mission was set up during 10:00 – 12:00 (JST) on April 23, 2016, which produced point clouds with an average point density of 3-4 points/m^2. Both sets of Lidar data were acquired using a Leica ALS50II instrument and the same pilot and airplane. After rasterization of the raw point clouds, two digital surface models (DSMs) with a data spacing of 50 cm were created. **Figure 2** shows the extent of the post-event DSM, which represents the entire study area. It covers the main part of Mashiki Town and some parts of Nishihara Village, Mifune and Kashima Towns, and Kumamoto City.

The study area is located in the near field of the Kumamoto earthquake sequence where significant permanent ground displacements were produced during the earthquake. A direct comparison of the pre- and post-event DSMs shows that

the building coordinates do not match because the post-DSM contains coseismic displacements. Therefore, the post-DSM was shifted before detecting the damaged buildings based on the permanent crustal movement [14]. **Figure 3** illustrates the calculated coseismic displacement for the common Lidar data area. The results of new field measurement carried out in August 2016 for surveying reference points after the Kumamoto Earthquake are also shown [17]. The coseismic displacements estimated from the Lidar data show good agreement with the survey results.

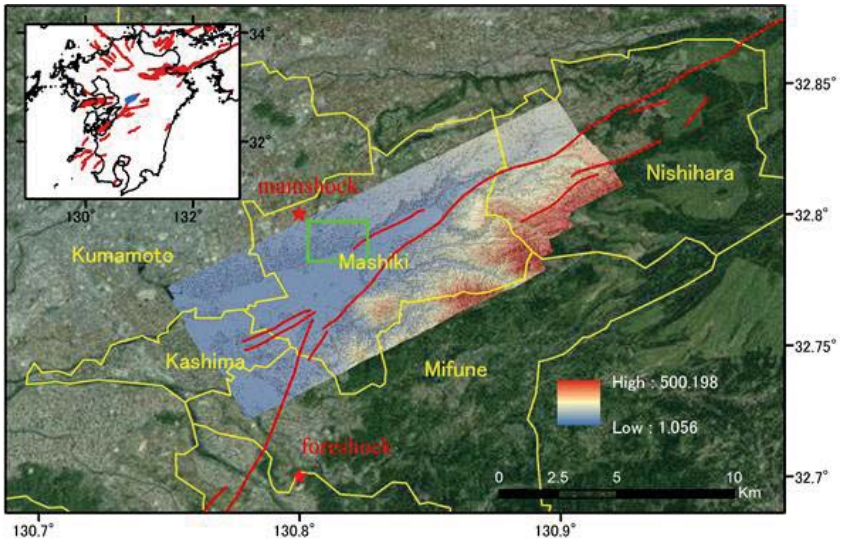

Figure 2. Location of the post-event Lidar data in Kumamoto Prefecture, Japan. Shaded colors represents the ground elevation. The green rectangle shows the locations of the central part of Mashiki Town, investigated in this study. The blue polygon in the inset depicts the study area.

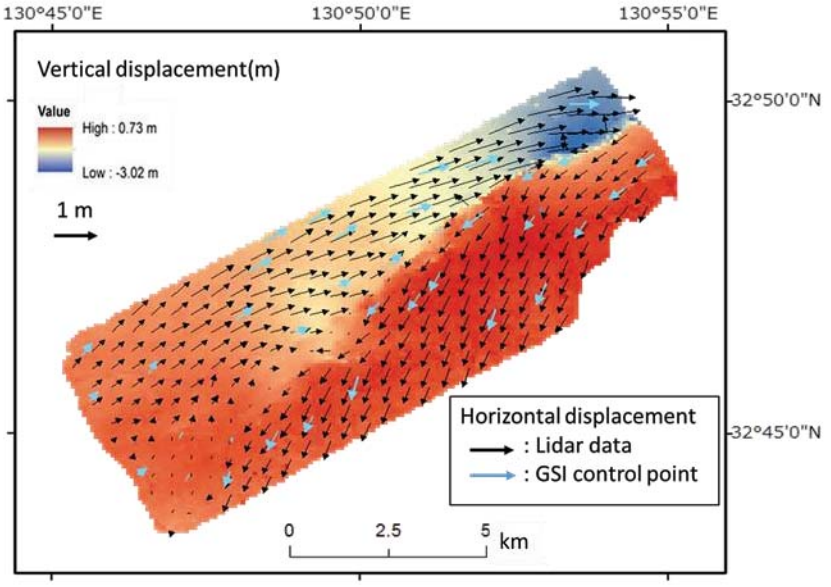

Figure 3. Estimated 3D coseismic displacement after the main-shock of the 2016 Kumamoto earthquake. The black arrows and shaded colors indicate the horizontal and vertical displacements obtained from the Lidar data, respectively [14]. The blue arrows indicate the horizontal displacements at the control points measured by the Geospatial Information Authority of Japan [17].

4. EXTRACTION OF COLLAPSED BUILDINGS

To focus on buildings, a geocoded building footprint dataset, provided by the Geospatial Information Authority of Japan (GSI), was used. Only buildings with footprint areas greater than 20 m^2 were evaluated. Because the point densities of the two DSMs are different and the footprint data include some errors, perfect matching of the DSMs with the building footprints could not be achieved. For this reason, the building footprints were reduced by 1 m. The LiDAR data within the reduced building boundaries were then extracted and processed. The reason for using the reduced building boundaries was to discard the DSM data near the building's boundaries in the subsequent analysis.

Figure 4 illustrates three buildings located in the study area. For each case, the pre-DSM (blue dots), the post-DSM (red dots), and the difference of the two DSMs are depicted. These buildings were selected in order to demonstrate different damage patterns: non-damaged, tilted, and collapsed buildings. It is worth noting that the difference between the DSMs for a non-collapsed building (**a**) shows high values around the boundary of the building footprint, which was caused by the effect mentioned earlier. These errors are certainly present for tilted buildings as well (**b**). **Figure 4c** shows a typical mid-story collapsed steel-frame building, in which the two DSMs and their difference highlight the damage pattern.

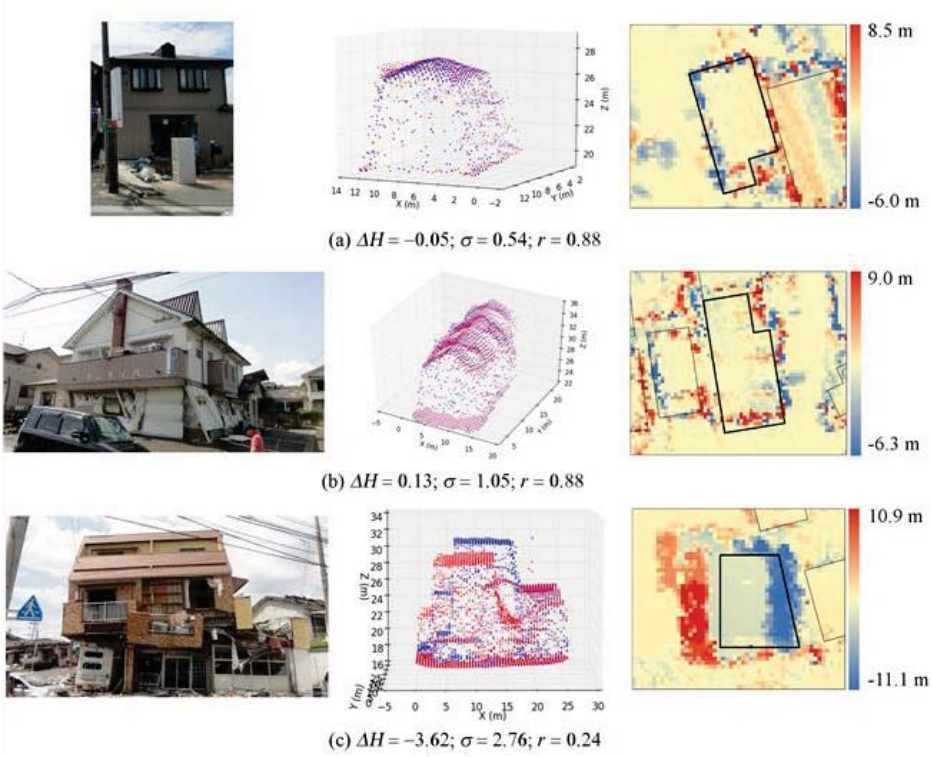

Figure 4. Examples of non-collapsed (a) and collapsed (b, c) buildings extracted using the Lidar DSM data. The left figure shows the photos taken after the main-shock by the authors, the middle figure the two Lidar DSMs, and the right figure the elevation differences between the two DSMs.

Figure 5 shows the relative vertical displacement calculated from the two Lidar DSMs, where blue colored pixels show the decrease of height, mostly due to the collapse of buildings. **Figure 6** shows the relationship between the height difference and the extracted area exceeding the plus and minus thresholds. For example, if 0.5-m is selected as the height difference threshold, about 8.5 % of the target area is extracted. Note that although the Lidar DSMs have elevation accuracy of less than 10 cm, the location accuracy of laser cloud points is an order of 50 – 70 cm. Considering this situation, +0.5 m was determined as the height difference threshold of changes for 0.5-m square grid Lidar data. It is recognized from the figure that the area of reduced-height pixels is about 1.6 times of the area of increased-height pixels. This observation can be explained by the fact that the reduced-height in this urban area is mostly due to the collapse of buildings and the increased-height is due to the accumulation of debris and the displacement of collapsed buildings to surrounding areas.

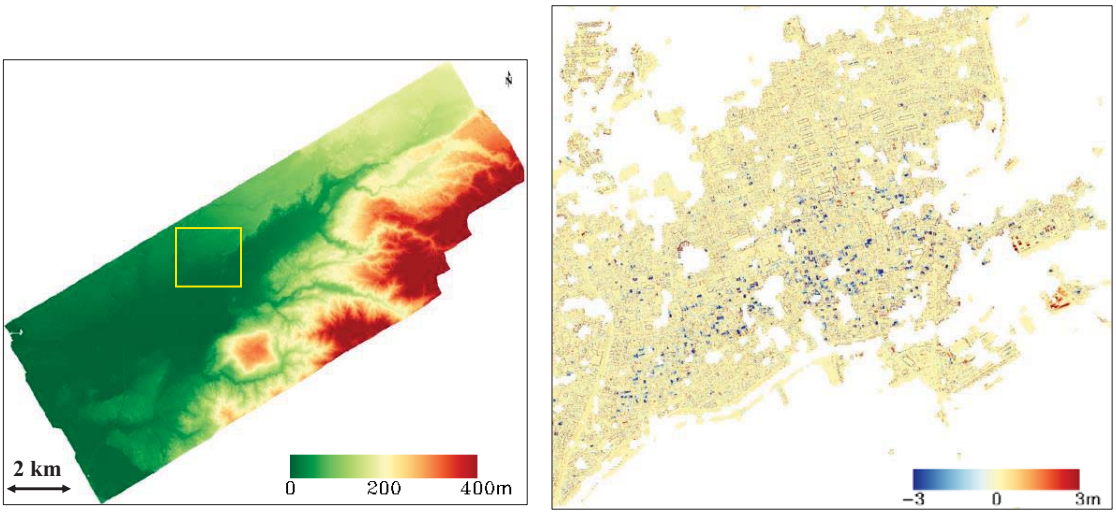

(a) (b)

Figure 5. DSM obtained from Lidar flight on April 23, 2016 (a) and the difference of the two DSMs' heights in the area shown by yellow square after removing crustal movements (b).

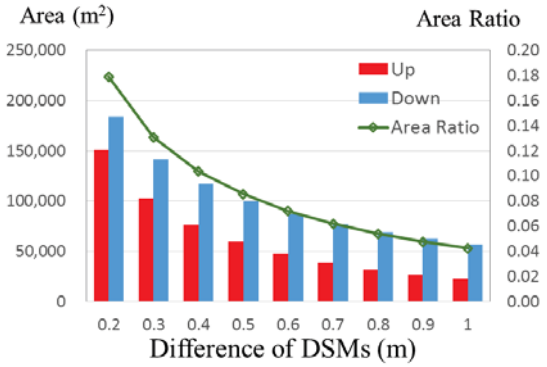

Figure 6. Relationship between the height difference and the area exceeding the plus and minus thresholds

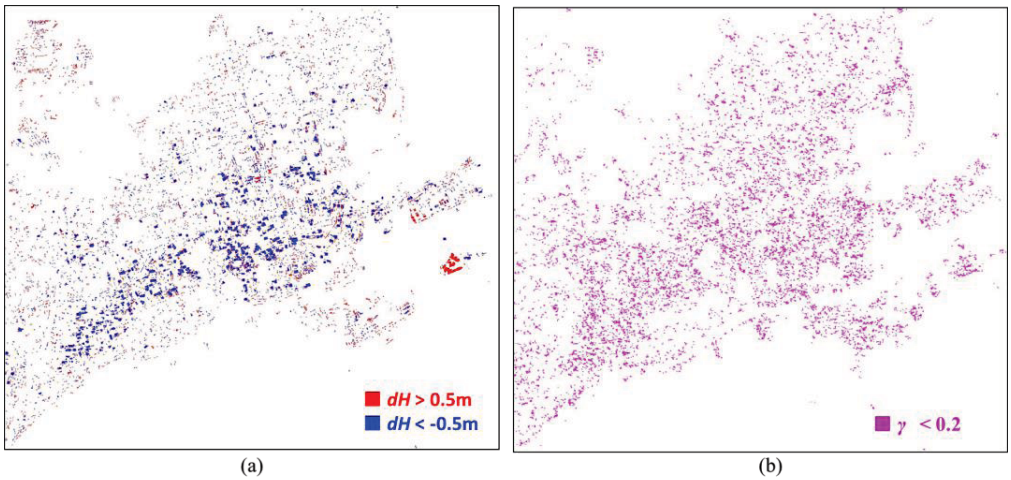

(a) (b)

Figure 7. Changed areas extracted by height-difference (abs. (dH) > 0.5 m) of the two DSMs (**a**); and changed areas extracted by low coherence ($\gamma < 0.2$) from PALSAR-2 data (**b**). Objects smaller than 9.0 m^2 were excluded as noises from these plots.

Figure 7 compares the possible changed areas extracted by height-difference (dH > 0.5 m or dH < -0.5 m) and those by low coherence ($\gamma < 0.2$) from pre- and post-event ALOS-2 PALSAR-2 data [18]. In these extractions, the objects smaller than 9.0 m^2 were removed as noises, such as cars and debris. The distributions of the extracted areas were not the same but very similar although the situations of change for the two data sets have some different aspects.

The extracted areas from the Lidar DSMs were closely examined for the central part of Mashiki Town including the town office building as shown in **Figure 8**. It is seen from the figure that by increasing the height-threshold, the selected areas are seen to decrease. Increased-height pixels are seen to be mostly parking cars and some debris while decreased-height pixels are collapsed buildings.

From all the comparisons, the most suitable threshold value of the average height reduction within a reduced building footprint was determined as 0.5 m [19]. **Figure 9** illustrates the spatial distribution of collapsed buildings estimated using this threshold for the entire study area, in which a large number of collapsed buildings were observed. The red and black polygons represent the collapsed (D5) and non-collapsed (D0-D4) buildings, respectively. The color of the pixels represents the difference in elevations between the two DSMs. Blue pixels depict the differences of elevations less than -0.5 m, and yellow pixels represent differences greater than 0 m. Within the study area, a total of 26,128 buildings were evaluated, and 1,760 buildings were classified as collapsed (dH less than -0.5 m).

Finally, **Figure 9b** provides a closer look of the areas where the collapsed buildings are concentrated, together with the location of the collapsed buildings surveyed by Yamada et al. [20] as black triangles. Note that the area of field survey was much smaller than our study area; it covers only the area with black triangles exist. A good agreement can be observed between the survey data and the DSM-based collapsed building extraction. Thus multi-temporal Lidar data is considered to be very effective to extract heavily impacted urban areas due to natural disasters.

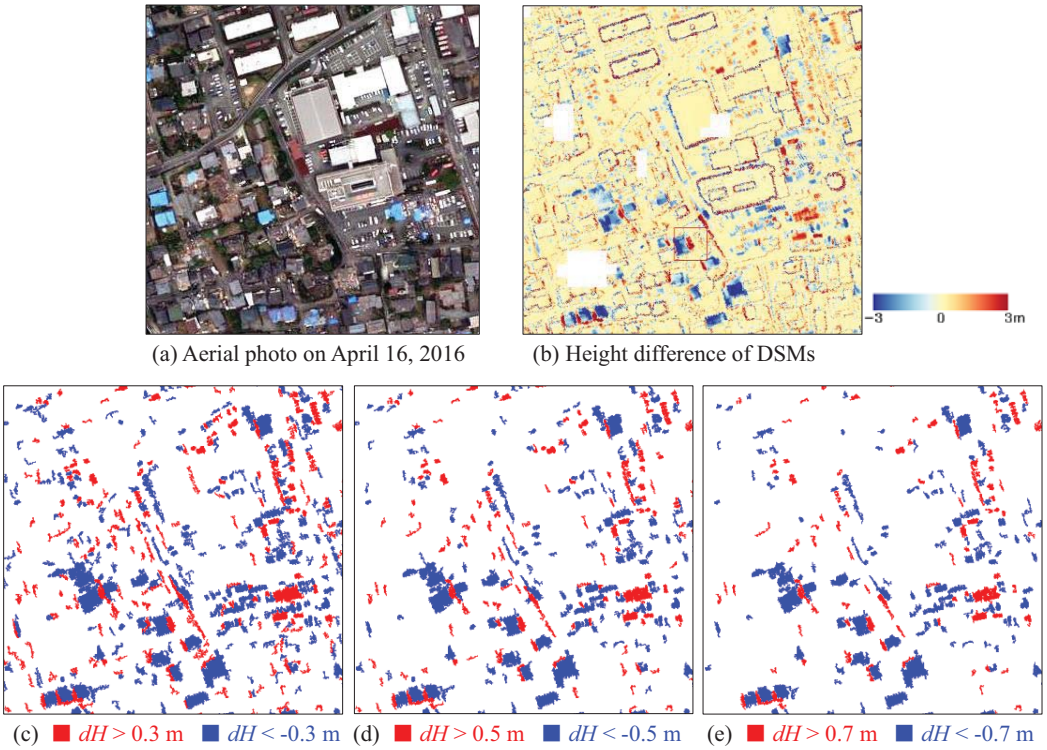

Figure 8. Aerial photograph around Mashiki Town office (a), height difference of the two DSMs (b), and extracted areas by different height-difference values (c-e). Objects smaller than 9.0 m^2 were excluded.

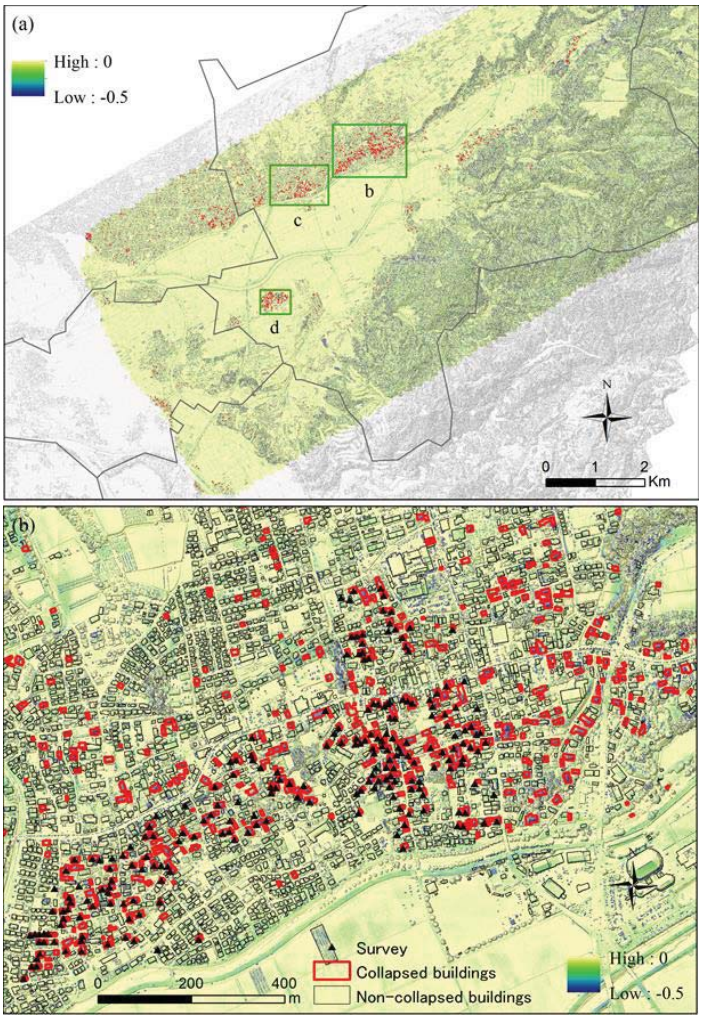

Figure 9. Map showing the distribution of collapsed buildings, shown as red polygons, in the entire study area [19]. The pixel color represents the difference in elevations between the two DSMs (a). The green squares show the location of area shown in (b). Close-up of Area b where the collapsed buildings were concentrated (b). The black triangles show the collapsed buildings from Yamada et al. [20].

5. CONCLUSIONS

Extraction of collapsed buildings from a pair of Lidar data taken before and after the 2016 Kumamoto, Japan, earthquake was attempted. The spatial correlation coefficient of the two Lidar data was calculated and the horizontal shift of the April-23 digital surface model (DSM) with the maximum correlation coefficient was considered as the crustal movement by the April-16 main-shock. The horizontal component of the calculated coseismic displacement was applied to the post-event DSM to cancel it, and then the vertical displacement between the two DSMs was calculated. The both horizontal and vertical coseismic displacements were removed to extract collapsed buildings. Then building-footprints were employed to assess the changes of the DSMs within them. The average of differences between the pre- and post-event DSMs within a building footprint was selected as a parameter to evaluate whether a building is collapsed or not. The extracted height difference values were compared with the spatial coherence values calculated from pre- and post-event ALOS-2 PALSAR-2 data. The comparison result indicates that the collapsed building can be extracted by setting a proper threshold value, plus and minus 0.5 m within a building footprint, and the selected total areas were closed to low coherence ($\gamma < 0.2$) areas from the pre- and post-event PALSAR-2 data. This conclusion was further validated by the result of field damage investigation.

ACKNOWLEDGMENT

This study was financially supported by a Grant-in-Aid for Scientific Research (Project numbers: 17H02066, 24241059) and the Core Research for Evolutional Science and Technology (CREST) program by the Japan Science and Technology Agency (JST) "Establishing the most advanced disaster reduction management system by fusion of real-time disaster simulation and big data assimilation (Research Director: Prof. S. Koshimura of Tohoku University)". The Lidar data used in this study were acquired and owned by Asia Air Survey Co., Ltd., Japan.

REFERENCES

[1] Yamazaki, F. and Matsuoka, M. "Remote sensing technologies in post-disaster damage assessment," Journal of Earthquakes and Tsunamis, 1(3), 193-210 (2007).

[2] Rathje, E., and Adams, B.J., "The role of remote sensing in earthquake science and engineering, opportunities and challenges," Earthquake Spectra, 24(2), 471–492 (2008).

[3] Eguchi, R.T., Huyck, C., Ghosh, S., Adams, B.J., "The application of remote sensing technologies for disaster management," The 14th World Conference on Earthquake Engineering, 17p (2008),.

[4] Brunner, D., Lemoine, G., Bruzzone, L., "Earthquake damage assessment of buildings using VHR optical and SAR imagery," IEEE Transactions on Geoscience and Remote Sensing, 48(5), 2403-2420 (2010).

[5] Dell'Acqua, F. and Gamba, P.. "Remote sensing and earthquake damage assessment: Experiences, limits, and perspectives," Proceedings of the IEEE 100 (10), 2876-2890 (2012).

[6] Liu, W., Yamazaki, F., Gokon, H., Koshimura, S., "Extraction of tsunami-flooded areas and damaged buildings in the 2011 Tohoku-Oki Earthquake from TerraSAR-X intensity images," Earthquake Spectra, 29(S1), S183-S200, (2013).

[7] Nakmuenwai, P., Yamazaki, F., Liu, W., "Automated extraction of inundated areas from multi-temporal dual-polarization RADARSAT-2 images of the 2011 central Thailand flood," Remote Sensing, 9(1), 78 (2017).

[8] Yamazaki, F., Bahri, R., Liu, W., Sasagawa, T., "Damage extraction of buildings in the 2015 Gorkha, Nepal earthquake from high-resolution SAR data," Proc. of SPIE, Vol. 9877, 98772K-1-11 (2016).

[9] Yamazaki, F., Suzuki, D., Maruyama, Y., "Use of digital aerial images to detect damages due to earthquakes," Proc. 14th World Conf. Earthquake Engineering, Paper No. 01-1049 (2008).

[10] Vu, T.T., Yamazaki, F. and Matsuoka, M., "Multi-scale solution for building extraction from LiDAR and image data," International Journal of Applied Earth Observation and Geoinformation, 11, 281–289 (2009).

[11] Cabinet Office of Japan, "Summary of damage situation in the Kumamoto earthquake sequence (in Japanese)," http://www.bousai.go.jp/updates/h280414jishin/index.html (accessed on 4 August 2017).

[12] Yamazaki, F. and Liu, W., "Remote sensing technologies for post-earthquake damage assessment: A case study on the 2016 Kumamoto earthquake," Keynote Lecture, 6th Asia Conference on Earthquake Engineering, Cebu City, Philippines, 8p (2016).

[13] Asia Air Survey Co., Ltd., "The 2016 Kumamoto earthquake, http://www.ajiko.co.jp/article/detail/ID5725UVGCD/ (accessed on 4 August 2017).

[14] Moya, L., Yamazaki, F., Liu, W., Chiba, T., "Calculation of coseismic displacement from lidar data in the 2016 Kumamoto, Japan, earthquake," Natural Hazards and Earth System Sciences, 17, 143-156 (2017).

[15] Japan Meteorological Agency, "The number of aftershocks of recent inland earthquakes in Japan," http://www.data.jma.go.jp/svd/eqev/data/2016_04_14_kumamoto/kaidan.pdf (accessed on 4 August 2017).

[16] Geospatial Information Authority of Japan, "the 2016 Kumamoto Earthquake (in Japanese)," http://www.gsi.go.jp/BOUSAI/H27-kumamoto-earthquake-index.html (accessed on 4 August 2017).

[17] Geospatial Information Authority of Japan, "New measurement for survey reference points after the 2016 Kumamoto Earthquake," http://www.gsi.go.jp/sokuchikijun/sokuchikijun60019.html (accessed on 4 August 2017).

[18] Liu, W. and Yamazaki, F., "Extraction of collapsed buildings due to the 2016 Kumamoto earthquake based on multi-temporal PALSAR-2 data," Journal of Disaster Research, 12(2), 241-250 (2017).

[19] Moya, L., Yamazaki, F., Liu, W., Yamada, M., "Detection of collapsed buildings due to the 2016 Kumamoto, Japan, earthquake from Lidar data," Natural Hazards and Earth System Sciences: Discussions, https://doi.org/10.5194/nhess-2017-186 (2017)

[20] Yamada, M., Ohmura, J., and Goto, H., "Wooden building damage analysis in Mashiki town for the 2016 Kumamoto earthquakes on April 14 and 16," Earthquake Spectra, *accepted for publication* (2017).